Molecular Biology of the Cell
Vol. 19, 2777–2788, July 2008

The Subcellular Distribution of Calnexin Is Mediated by PACS-2

Nathan Myhill,* Emily M. Lynes,* Jalal A. Nanji,* Anastassia D. Blagoveshchenskaya,†‡ Hao Fei,†§ Katia Carmine Simmen,†‖ Timothy J. Cooper,* Gary Thomas,† and Thomas Simmen*†

*Department of Cell Biology, University of Alberta, Edmonton, Alberta, T6G2H7, Canada; and †Vollum Institute, Oregon Health and Science University, Portland, OR 97239

Submitted October 3, 2007; Revised March 28, 2008; Accepted April 9, 2008
Monitoring Editor: Adam Linstedt

Calnexin is an endoplasmic reticulum (ER) lectin that mediates protein folding on the rough ER. Calnexin also interacts with ER calcium pumps that localize to the mitochondria-associated membrane (MAM). Depending on ER homeostasis, varying amounts of calnexin target to the plasma membrane. However, no regulated sorting mechanism is so far known for calnexin. Our results now describe how the interaction of calnexin with the cytosolic sorting protein PACS-2 distributes calnexin between the rough ER, the MAM, and the plasma membrane. Under control conditions, more than 80% of calnexin localizes to the ER, with the majority on the MAM. PACS-2 knockdown disrupts the calnexin distribution within the ER and increases its levels on the cell surface. Phosphorylation by protein kinase CK2 of two calnexin cytosolic serines (Ser554/564) reduces calnexin binding to PACS-2. Consistent with this, a Ser554/564 → Asp phosphomimic mutation partially reproduces PACS-2 knockdown by increasing the calnexin signal on the cell surface and reducing it on the MAM. PACS-2 knockdown does not reduce retention of other ER markers. Therefore, our results suggest that the phosphorylation state of the calnexin cytosolic domain and its interaction with PACS-2 sort this chaperone between domains of the ER and the plasma membrane.

INTRODUCTION

A principal function of the ER is chaperone-mediated oxidative folding of newly synthesized proteins, thought to occur close to the translocon on the rER with the help of chaperones (Chen and Helenius, 2000). Recent research has started to view the ER as a multifunctional organelle that comprises distinct domains devoted to specific tasks. Examples are oxidative protein folding that occurs on the rough ER (rER) or lipid synthesis that is associated with the mitochondria-associated membrane (MAM; Vance, 1990; Borgese *et al.,* 2006; Levine and Loewen, 2006). It is also emerging that many ER proteins, including chaperones, localize to multiple ER membrane domains, where they perform distinct functions. Examples are the chaperones calnexin (CNX), calreticulin and ERp44, which interact with the MAM-enriched IP_3R and SERCA2b, respectively (John *et al.,* 1998; Roderick *et al.,* 2000; Higo *et al.,* 2005).

Coat- and receptor-based retention and retrieval mechanisms ensure that ER folding chaperones and oxidoreductases localize to the ER (Teasdale and Jackson, 1996; Duden, 2003; Michelsen *et al.,* 2005). However, in addition to multiple domains of the ER, many ER chaperones such as BiP/GRP78, PDI , and CNX have also been found on the plasma membrane, suggesting that their intracellular retention and trafficking along the secretory pathway varies (Wiest *et al.,* 1995; Mezghrani *et al.,* 2000; Arap *et al.,* 2004; Misra *et al.,* 2006). For instance, high levels of CNX characterize the plasma membrane of immature thymocytes. Conversely, ER stress can reduce surface CNX (Wiest *et al.,* 1995; Okazaki *et al.,* 2000). Changing the amount of CNX on the plasma membrane could affect cell surface properties and might have implications on phagocytosis or cell–cell interactions (Gagnon *et al.,* 2002). Hence, the amount of CNX on the plasma membrane could depend on the cell type or cellular homeostasis, and it might be the result of regulated intracellular retention.

In addition to folding intermediates, ribosomes and SERCA2b, CNX also interacts with BAP31, an ER cargo receptor that mediates export of transmembrane proteins from the ER and shuttles them to the ER quality control compartment (Annaert *et al.,* 1997; Spiliotis *et al.,* 2000; Kamhi-Nesher *et al.,* 2001; Zuppini *et al.,* 2002; Frenkel *et al.,* 2004; Zen *et al.,* 2004; Groenendyk *et al.,* 2006; Wakana *et al.,* 2008). The only functional significance that has so far been attributed to this interaction is a regulation of caspase cleavage of BAP31 during the onset of apoptosis (Zuppini *et al.,* 2002;

This article was published online ahead of print in *MBC in Press* (http://www.molbiolcell.org/cgi/doi/10.1091/mbc.E07–10–0995) on April 16, 2008.

Present addresses: ‖Department of Biochemistry, University of Alberta, Edmonton, AB, T6G 2H7, Canada; §Department of Psychiatry and Biobehavioral Sciences, The David Geffen School of Medicine at UCLA, Los Angeles, CA 90095; ‡Department of Medicine, Division of Nephrology and Hypertension, Oregon Health and Science University, Portland, OR 97239.

Address correspondence to: Thomas Simmen (Thomas.Simmen@ualberta.ca).

Abbreviations used: BAP31, B-cell receptor associated protein of 31 kDa; CI-MPR, cation-independent mannose 6-phosphate receptor; CK2, protein kinase CK2; CNX, calnexin; COPI, coatomer; ER, endoplasmic reticulum; ERK, extracellular signal regulated kinase; MAM, mitochondria-associated membrane; PACS-2, phosphofurin acidic cluster sorting protein 2, PDI, protein disulfide isomerase; rER, rough endoplasmic reticulum

Breckenridge *et al.*, 2003; Groenendyk *et al.*, 2006). It is not known whether BAP31 can influence the intracellular targeting of CNX.

In summary, CNX can reach the plasma membrane and can also interact with numerous ER membrane proteins that are found on multiple domains of the ER such as the MAM. Although CNX and other ER chaperones clearly localize to multiple cellular membranes, it is currently not understood whether the cell has mechanisms in place that control the distribution of chaperones between these various locations.

Support for the hypothesis of a controlled distribution of ER proteins to specific membrane domains comes from pioneering studies on CNX (Chevet *et al.*, 1999; Roderick *et al.*, 2000). These articles showed that protein kinase C (PKC), extracellular-signal regulated kinase-1 (ERK-1) and protein kinase CK2 (CK2) can phosphorylate the CNX cytosolic domain. Phosphorylation by ERK-1 on serine 583 increases interaction of CNX with ribosomes, but also interaction with SERCA2b. In addition, CK2 phosphorylation of serines 554 and 564 by CK2 synergizes with ERK-1 phosphorylation of serine 583 to promote interaction with ribosomes (Chevet *et al.*, 1999). Hence, the CNX phosphorylation state could lead to enrichment on the MAM and the rER, where these CNX interactors are found. However, it is still unclear what happens to dephosphorylated CNX that has been demonstrated to exist in vivo (Wong *et al.*, 1998).

The CK2 site of CNX, but not the ERK-1 site, is embedded within an acidic cluster (see Figure 1A). Interestingly, CK2-phosphorylatable acidic clusters are hallmark interaction sequences for proteins of the PACS family, which includes PACS-1 and PACS-2 (Wan *et al.*, 1998; Kottgen *et al.*, 2005; Simmen *et al.*, 2005; Feliciangeli *et al.*, 2006; Scott *et al.*, 2006). The interaction of these acidic motifs with PACS proteins mediates a variety of intracellular targeting steps that include trafficking between the *trans*-Golgi (TGN) network and endosomes, localization to mitochondria and retention in the ER. Cargo proteins can usually interact with both PACS-1 and PACS-2 (Kottgen *et al.*, 2005; Feliciangeli *et al.*, 2006). The intracellular targeting that results from the cargo protein–PACS interaction is typically influenced by the formation of ternary complexes with additional proteins that include coatomer (COPI), adaptor proteins, and even CK2 itself (Crump *et al.*, 2001; Kottgen *et al.*, 2005; Scott *et al.*, 2006; Atkins *et al.*, 2008). Phosphorylation by CK2 on serines associated with the acidic motifs often serves as a switch that either promotes or blocks interaction with PACS proteins (Schermer *et al.*, 2005; Scott *et al.*, 2006).

The multifunctional cytosolic sorting protein PACS-2 interacts with COPI and controls the ER localization of transmembrane proteins such as polycystin-2 or profurin with a cytosolic CK2-phosphorylatable acidic cluster (Kottgen *et al.*, 2005; Feliciangeli *et al.*, 2006). PACS-2 also mediates the sorting of internalized cation-independent mannose 6-phosphate receptor (CI-MPR) from early endosomes to the TGN and interacts with HIV-1 Nef to assemble a multikinase cascade that triggers MHC-I down-regulation (Atkins *et al.*, 2008). Moreover, PACS-2 promotes MAM integrity and regulates its composition (Simmen *et al.*, 2005). Because the MAM harbors the machinery for calcium communication between the ER and mitochondria during the onset of apoptosis (Rizzuto *et al.*, 1998; Goetz *et al.*, 2007), knockdown of PACS-2 reduces both ER–mitochondria calcium exchange and apoptosis triggering (Simmen *et al.*, 2005).

Here, we identify CNX as a novel PACS-2 cargo protein on the ER. CNX interacts with PACS-2 using its acidic CK2 motif. Although this sequence in its phosphorylated form increases interaction with ribosomes (Chevet *et al.*, 1999), our results show that the nonphosphorylated CK2 motif interacts with PACS-2, thus retaining CNX within the ER and promoting CNX localization to heavy membranes of the ER and to MAMs. This PACS-2 localization mechanism is specific, because the knockdown of PACS-2 does not significantly affect the membrane fractionation of ER proteins that lack the PACS-2 motif, such as BAP31, ribophorin-I, or PDI. It also does not lead to reduced ER retention of BAP31. Our results thus show how the phospho-regulated interaction of CNX with PACS-2 could result in its distribution between the plasma membrane, the rER, and the MAM. PACS-2 interaction thus determines the amounts of CNX available for interaction with ribosomes on the rER and with SERCA2b on the MAM.

MATERIALS AND METHODS

Antibodies and Reagents

All chemicals were from Sigma (Oakville, ON, Canada). The PACS-1 and PACS-2 expressing viruses and rabbit anti-PACS-1 (601) and anti-PACS-2 (604) antibodies, have been described previously (Simmen *et al.*, 2005). The polyclonal antiserum against BAP31 was provided by G. Shore (Montréal, QC, Canada), and the monoclonal anti-biotin was a gift from Dr. L. Berthiaume (Edmonton, AB, Canada). The antibodies used were as follows: actin, BAP31, PDI, ribophorin-I, ACAT1, Sec61α, (Affinity BioReagents, Golden, CO); ERGIC53 (Alexis, Lausen, Switzerland); mitochondrial complex II (MitoSciences, Eugene, OR); thioredoxin (Invitrogen, Carlsbad, CA); CNX (polyclonal: Stressgen, Victoria, BC; monoclonal: BD Biosciences, Mississauga, ON, Canada); BiP (BD Biosciences, Mississauga, ON, Canada); β-COP (MaD, GeneTex, San Antonio, TX); GM-130 and caspase-3 (Cell Signaling, Danvers, MA); the FLAG tag (Rockland, Gilbertsville, PA); and the hemagglutinin (HA) tag (Covance, Berkeley, CA). CNX wild-type and knockout mouse embryonic fibroblasts (MEFs) were from M. Michalak (Edmonton, AB, Canada). HeLa cells were from ECACC (Porton Down, United Kingdom). Human and mouse PACS-2 small interfering RNAs (siRNAs; HSS146279, MSS211622) were from Invitrogen. All other siRNAs were previously described.

Expression Vectors and Mutagenesis

PACS-2 plasmids were previously described (Simmen *et al.*, 2005). The dog CNX cDNA was provided by E. Chevet (Montréal, QC, Canada). For glutathione *S*-transferase (GST) constructs, specific primers (Sigma) were used to generate tail mutations by PCR as indicated in the text. PCR products were inserted into pGEX4T1 (GE Healthcare, Baie d'Urfé, QC, Canada) using the BamHI and XhoI restriction sites. For mutagenesis of serines 554 and 564, we used the following oligos: TS157: GCAGATGCTGAAGAAGATGGCGGCACCGCGGCACAAGAGGAGGACGAT; TS158: GGTGCCGCCATCTTCTTCAGCATCTGCTTTTTGCTTCTCTTCAAGTTT; TS173: GCTGAAGAAGATGGCGGCACAGCTGATCAAGAGGAGGACGATAGG; and TS174: CAGCTGTGCCGCCATCTTCTTCAGCATCATCTTTTTGCTTCTCTTC.

FLAG-tagged CNX was constructed as follows: first, a lumenal FLAG tag was inserted by PCR right after the signal sequence. We used the following staggered primers: TS262: TACAAGGACGACGATGACAAGGGACATGAAGGACATGATGATGATATG; TS263: ATGTTACTGGTCCTTGGAACTACTATTGTTCAGGCTGACTACAAGGACGACGATGAC; and TS264: TATGGTACCACCATGGAAGGGAAATGGCTGCTGTGTATGTTACTGGTCCTTGGAACTAC.

Next, the mutagenesis oligos were used to recreate the GST mutants.

Immunofluorescence Microscopy, Transfections, and Western Blotting

Processing for immunofluorescence microscopy was performed as follows. Briefly, HeLa cells were grown on coverslips for 24 h (untransfected cells) or 72 h (when siRNA-transfected). Cells were washed with PBS containing 1 mM $CaCl_2$ and 0.5 mM $MgCl_2$ (PBS^{2+}) and fixed with 3% paraformaldehyde for 20 min. After washing with PBS^{2+}, cells were permeabilized for 1 min with 0.1% Triton X-100, 0.2% BSA in PBS^{2+}. Cells were then incubated with primary antibodies (1:100) and secondary antibodies in PBS^{2+}, 0.2% BSA for 1 h each, interrupted with three washes using PBS^{2+}. All secondary antibodies were AlexaFluor-conjugated 350, 488, or 546 (Invitrogen, Carlsbad, CA) used at 1:2000. After final washes, cells were mounted in ProLong Antifade (Invitrogen). Images were obtained with an Axiocam on an Axioobserver microscope (Carl Zeiss, Jena, Germany) using a 100× Plan-Apochromat lens. All images were iteratively deconvolved using the Axiovision 4 software. Stable transfections and Western blotting protocols were identical to Simmen *et al.* (1999, 2005). Transient transfection with siRNAs was identical to Simmen *et al.* (2005), and silenced cells were analyzed on the second day after knockdown, when knockdown of PACS-2 is maximal. Identification of PACS-2–depleted

cells for immunofluorescence took advantage of scoring for the characteristic fragmentation of mitochondria.

We performed radial profiling and analysis of exposures using the ImageJ software (http://rsb.info.nih.gov/ij/) and its Interactive 3D Surface Plot plug-in. Briefly, immunofluorescence images used for this article were split into RGB and transformed into a 3D heat map as seen on Supplemental Figure S2A and processed equally. Equal exposure corresponds to equal color profiles. The radial decrease of the immunofluorescence signals for CNX and BAP31 was measured as the percentage of the distance from the maximum signal to the minimum signal on a straight line (n = 8 images).

Membrane Fractionation, Protein–Protein Binding, and Biotinylation Assays

The membranes that constitute the ER and the Golgi were fractionated on a continuous Optiprep gradient (Axis-Shield, Dundee, Scotland) using 25, 20, 15, 10, and 5% Optiprep. HeLa cells, treated as indicated, were harvested in homogenization buffer (0.25 M sucrose, 10 mM HEPES-NaOH, pH 7.4, 1 mM EDTA) and passed 15 times through a ball-bearing homogenizer (Isobiotec, Heidelberg, Germany) with 18-μm clearance. Cell debris and nuclei were pelleted by centrifugation at 1000 $\times$ g for 10 min. The postnuclear supernatant was overlayed onto the continuous gradient and centrifuged at 32,700 rpm for 3 h at 4°C. Six equal fractions were collected from the top of the gradient and precipitated with acetone. Fractions were probed on a Western blot for CNX, β-COP, surface biotinylated proteins, mitochondrial complex II, and ribophorin I.

Heavy and light membranes were separated as follows: The cells were homogenized as above, and the resulting cell lysates were centrifuged for 10 min at 800 $\times$ *g* to remove unbroken cells and nuclei. Postnuclear lysates were centrifuged for 10 min at 10,000 $\times$ *g* to yield heavy membrane fractions (HM). The supernatants were then centrifuged for 60 min at 100,000 $\times$ *g* to separate cytosolic fraction (Cyt.) and light membrane fractions (LM). The in vitro–binding assay and surface biotinylations were performed as previously described (Simmen *et al.*, 2005). We determined the amount of surface CNX by comparing 5% of the total lysates to 100% of the biotinylated samples (see inset Figure 3D). The integrity of the ER was assayed with anti-ribophorin I antibodies (Affinity BioReagents).

Coimmunoprecipitation

For the CNX/HA-PACS-2 coimmunoprecipitation, plasmid transfected HeLa cells were harvested in m-RIPA (1% NP40, 1% deoxycholine, 150 mM NaCl, 50 mM Tris, pH 8.0, Complete protease inhibitors; Roche, Basel, Switzerland). HA-tagged PACS-2 was immunoprecipitated with anti-HA mAb HA.11. All antibodies were precipitated with protein A Sepharose (GE Healthcare, Baie d'Urfé, QC, Canada). Western blots were probed with an anti-HA and anti-CNX antibody.

RESULTS

PACS-2 Interacts with CNX

The interaction of CNX with ribosomes and SERCA2b depends on the ERK-1/PKC phosphorylation state of serine 583 in its cytosolic domain (Chevet *et al.*, 1999; Roderick *et al.*, 2000; Figure 1A). Additionally, CK2 phosphorylation of serines 554 and 564 acts synergistically with serine 583 phosphorylation to promote ribosome interaction. Because the two CK2 phosphorylation sites are embedded within an acidic cluster that is the PACS protein-binding consensus, we hypothesized that CNX may interact with PACS family sorting proteins (Wan *et al.*, 1998; Kottgen *et al.*, 2005; Simmen *et al.*, 2005; Feliciangeli *et al.*, 2006; Scott *et al.*, 2006). Consistent with this possibility, we found that under resting conditions, the PACS-2 staining pattern partially overlapped with CNX and mitochondria. In addition, some of the areas containing both CNX and PACS-2 also overlapped with mitochondria, suggesting that the two proteins can be found on the same membrane domains (Figure 1B, red arrowheads).

Based on the colocalization of PACS-2 and CNX, we next tested whether CNX and PACS-2 interact (Figures 2, A–D). Most proteins that interact with PACS proteins not only interact with PACS-2, but also with PACS-1. Two examples are profurin and polycystin-2. Although PACS-2 interaction mediates their retention within the ER, PACS-1 interaction regulates their trafficking at the TGN and endosomal level

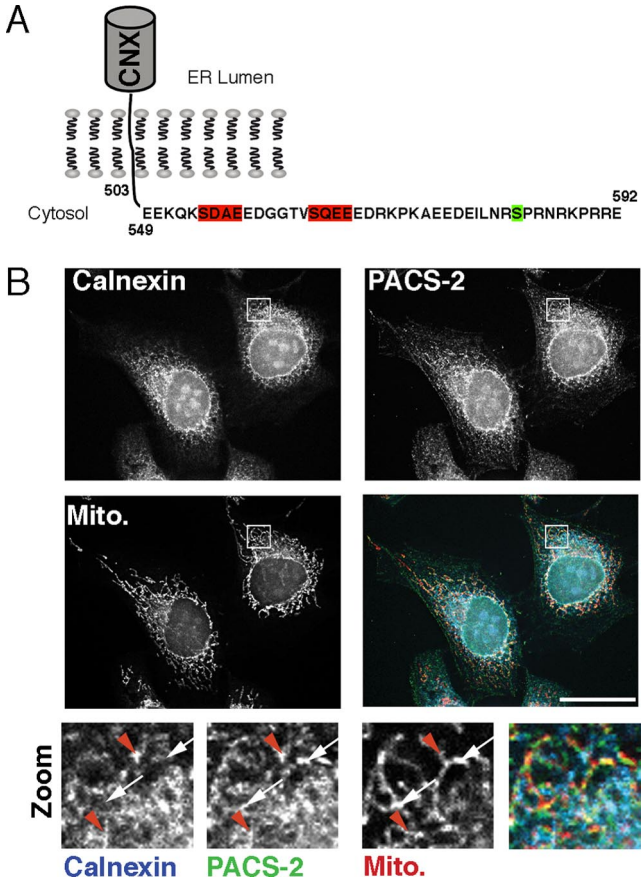

Figure 1. Identification of CNX, a potential interactor for PACS-2. (A) Schematic of dog CNX cytosolic domain. CK2 sites at residues 554 and 564 are highlighted in red, whereas the ERK-1 site at residue 583 is indicated in green. (B) A portion of CNX colocalizes with PACS-2 in the vicinity of mitochondria. HeLa cells were grown on coverslips for 24 h and processed for immunofluorescence microscopy. CNX was detected with a mouse mAb (BD Biosciences), PACS-2 with a rabbit polyclonal antiserum (604) and mitochondria with preloaded Mitotracker. Bottom row, magnified area, indicated with the white frame on the overlay. White arrows, PACS-2/mitochondria overlap; red arrowheads, triple overlap. Scale bar, 25 μm.

(Kottgen *et al.*, 2005; Feliciangeli *et al.*, 2006). Therefore, we examined if CNX shows preferential interaction in a pull-down assay with either one of the PACS proteins. We incubated HA-tagged full-length PACS-1 and PACS-2 from cellular lysates with bacteria-produced GST-tagged CNX cytosolic fragments (GST-CNX). Unexpectedly, we found that GST-CNX pulled down about three times more PACS-2 than PACS-1 (Figure 2A). This interaction pattern distinguishes CNX from other PACS protein interactors and suggests that PACS-2 is more important for its intracellular routing than PACS-1. We next aimed to confirm the CNX/PACS-2 interaction by immunoprecipitation. For this purpose, we used lysates from HeLa cells transiently transfected with HA-tagged PACS-2 in pcDNA3 or the empty plasmid to immunoprecipitate PACS-2 and probe for associated CNX by Western blot. We were able to detect endogenous CNX under these conditions, thus confirming the PACS-2/CNX interaction (Figure 2B).

Binding of cargo to PACS-2 is typically regulated by protein kinase CK2 phosphorylation (Kottgen *et al.*, 2005; Simmen *et al.*, 2005). We therefore asked whether CK2 phosphorylation on serines 554 and 564 regulates CNX binding

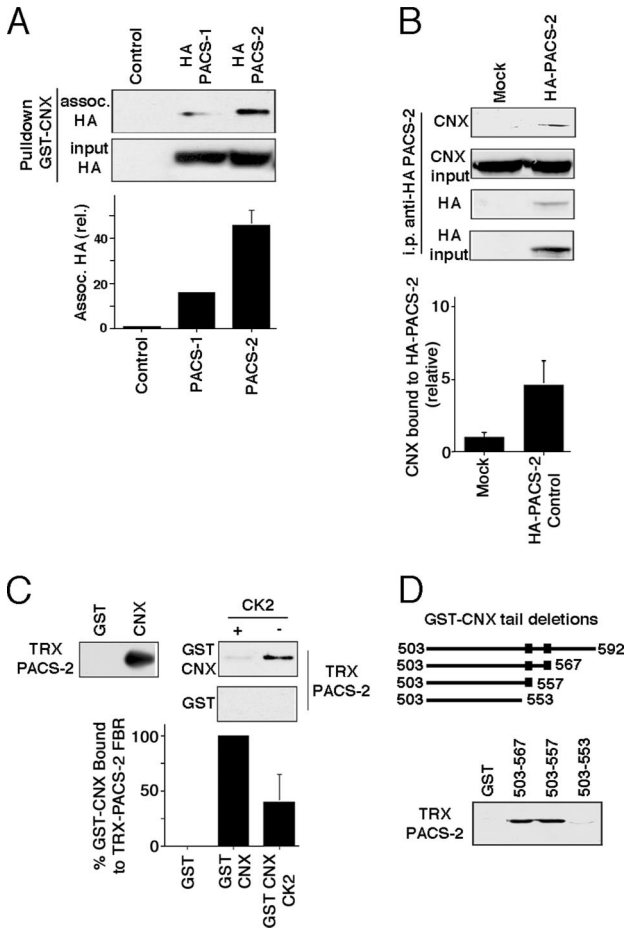

Figure 2. CNX interacts with PACS-2 dependent on its phosphorylation state. (A) Pulldown of transfected, tagged PACS proteins using the CNX cytosolic domain. HeLa cells were transfected or not with HA-tagged PACS-1 or PACS-2 in pcDNA3. The GST-tagged CNX cytosolic domain was used to pull down material. Associated proteins were assayed on a Western blot using an anti-HA antibody. Two independent experiments were quantified. (B) CNX/HA-PACS-2 coimmunoprecipitation. HeLa cells were transfected or not with HA-tagged PACS-2 in pcDNA3. Lysates were incubated with anti-HA monoclonal antibodies, and immunoprecipitates were analyzed for associated CNX by Western blot. Triplicates were quantified. (C) CNX in vitro binding. Left, detection of the binding of the thioredoxin (TRX)-tagged cargo-binding domain of PACS-2 (furin-binding region, FBR) to the GST-tagged CNX cytosolic tail, compared with the GST control. Right, TRX-PACS-2FBR was incubated with GST or GST-tagged CNX tail previously incubated or not with protein kinase CK2. Bound molecules were detected by Western blot using anti-GST antibodies. Equal loading was verified by Ponceau staining (data not shown). Three independent experiments were quantified. (D) CNX tail deletions. The diagram on top shows the deletions with their first and last residue, compared with wild-type CNX (top, 503–592). Also indicated with boxed symbols are the two CK2 sites. The gel shows the detection of the binding of thioredoxin (TRX)-tagged cargo-binding domain of PACS-2 (FBR) to GST-tagged CNX cytosolic tail deletions.

to PACS-2 (Figure 1A). We found that the thioredoxin-tagged cargo-binding domain of PACS-2 (TRX-PACS-2) bound preferentially to nonphosphorylated GST-CNX in vitro (Figure 2C). To determine which one of the CK2 sites is preferentially responsible for binding to PACS-2, we deleted portions from the CNX cytosolic domain and expressed these constructs as GST fusion proteins. Using these deletions, we determined that the presence of the membrane-proximal CK2 motif encompassing residues 554–557 is necessary for binding PACS-2 (Figure 2D).

Taken together our results show that a portion of PACS-2 and CNX colocalized in the vicinity of mitochondria and that PACS-2/CNX interaction can be observed in vitro and in vivo.

PACS-2 Controls the Intracellular Localization of CNX

Given the involvement of PACS-2 in ER localization, we asked if the CNX-PACS-2 interaction targets CNX to the ER and whether PACS-2 affects preferentially its interactor CNX or the entire ER. Thus, we first reexamined the intracellular localization of CNX in HeLa cells by immunofluorescence. In control cells transfected with a scrambled siRNA oligo, CNX showed a typical ER staining pattern that partially overlapped with mitochondria as shown in Figure 1B (see green arrowheads in Figure 3, A and B). Next, we silenced the PACS-2 gene by 2-d transient siRNA transfection and tested if this condition resulted in an altered staining for CNX. As previously reported, PACS-2 knockdown resulted in the formation of fragmented, often ring-shaped mitochondria (Supplemental Figure S1A, inset of Figure 3F; Simmen *et al.*, 2005). Concomitant with the alteration of the mitochondrial structure, the overlap between CNX and mitochondria disappeared almost completely in the cell periphery (Figure 3, E and F). Interestingly, CNX appeared collapsed in a juxtanuclear pattern, where interaction with mitochondria could in principle still happen, as most mitochondria are found there.

To determine whether the intracellular relocalization of CNX upon PACS-2 knockdown was specific, we compared its staining pattern to the one of BAP31, a known CNX interactor (Zuppini *et al.*, 2002). Under control conditions in cells transfected with a scrambled oligo, BAP31 showed a reticular staining pattern that showed extensive, albeit not perfect overlap with CNX (see red arrowheads in Figure 3, A and C). Both CNX and BAP31 also overlapped partially with mitochondria (see insets in Figure 3, A–D). In cells where PACS-2 had been silenced by 2-d transient siRNA transfection, BAP31 appeared concentrated to some extent in the juxtanuclear area, but still showed staining in the cell periphery, contrasting with the effect seen for CNX. Strikingly, BAP31 also maintained its overlap with mitochondria in the cell periphery (see insets in Figure 3, F and G). We confirmed this impression using radial profiling on cell surface heat maps that measure the gradient of individual staining and assess the exposure levels of our images (Supplemental Figure S2A). Although under control conditions in cells transfected with a scrambled siRNA oligo this gradient of staining was equal for CNX and BAP31, PACS-2 knockdown led to a sharper gradient of the CNX signal, but affected the BAP31 staining gradient only to a minor extent (Supplemental Figure S2B). These results suggest that PACS-2 localizes CNX to the peripheral portions of the ER. Conversely, PACS-2 knockdown affects BAP31 in a more subtle way. Although the overlap of the BAP31 signal with mitochondria is not reduced significantly by PACS-2 knockdown, BAP31 still concentrates in a juxtanuclear area in cells lacking PACS-2.

Because PACS-2 knockdown could potentially affect other organelles aside from mitochondria and from ER-localized CNX, we also examined the influence of PACS-2 knockdown on the Golgi complex and found that it had no significant effect, as previously reported (Supplemental Figure S1B and Kottgen *et al.*, 2005). Moreover, depletion of more than 90% of PACS-2 did not cause toxicity, as assayed with active

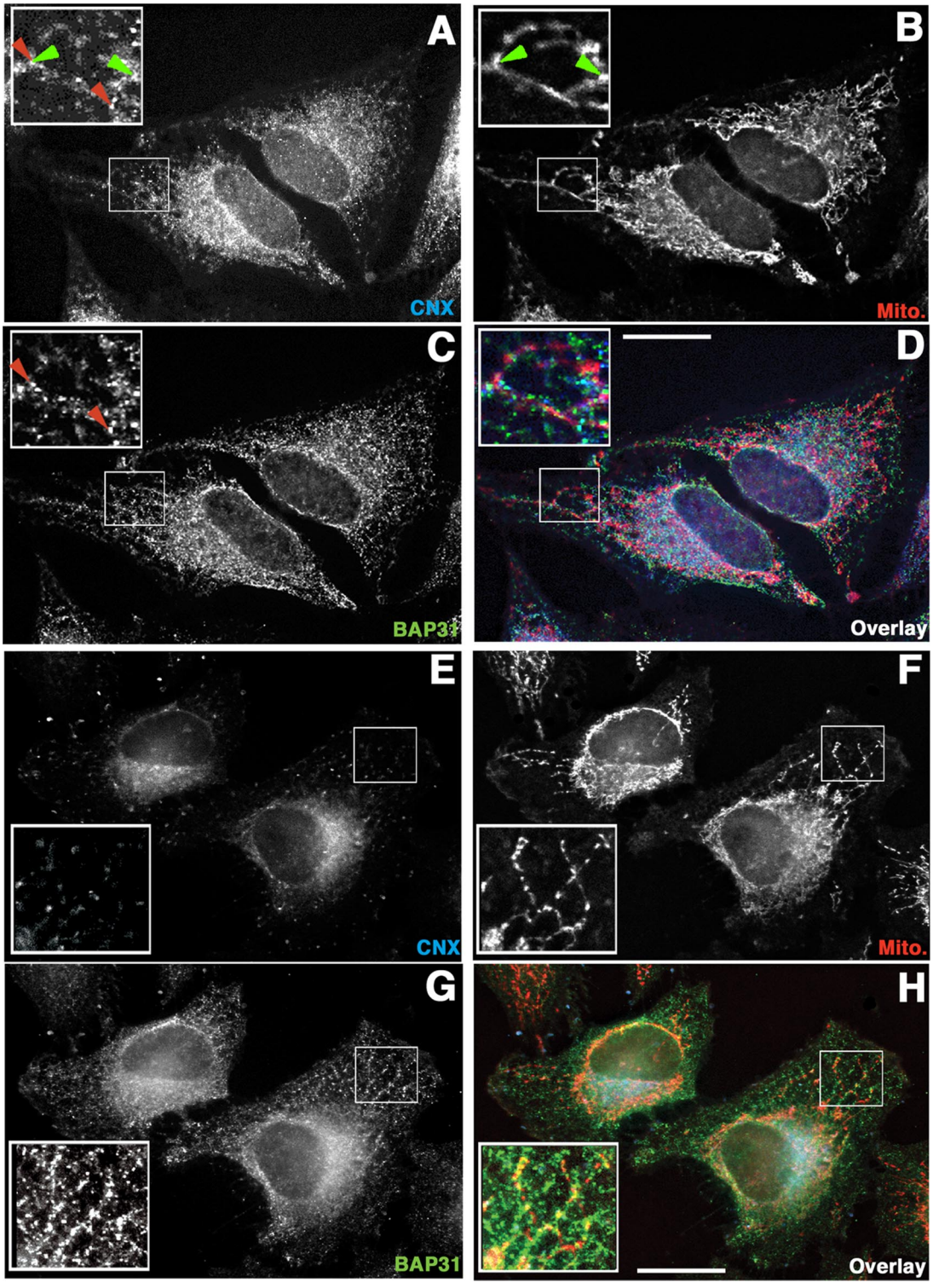

Figure 3. PACS-2 knockdown alters the CNX and mitochondria staining pattern, but affects BAP31 only marginally. Cells transfected with a scrambled oligo (A–D) and cells transfected with PACS-2 siRNA (E–H) were grown on coverslips and processed for immunofluorescence with anti-CNX (A and E), and anti-BAP31 antisera (C and G), after Mitotracker loading (B and F). Overlay pictures show all three markers (D and H). Insets show indicated magnifications. CNX overlap with mitochondria is indicated by green arrowheads, whereas CNX overlap with BAP31 is indicated by red arrowheads. PACS-2–depleted cells were identified by the characteristic mitochondrial fragmentation, as described in Simmen *et al.* (2005). Scale bar, 25 μm.

caspase-3, indicating that PACS-2 silenced cells are viable (Supplemental Figure S1C).

We next aimed to further characterize the CNX relocation upon PACS-2 knockdown. We asked whether the restriction

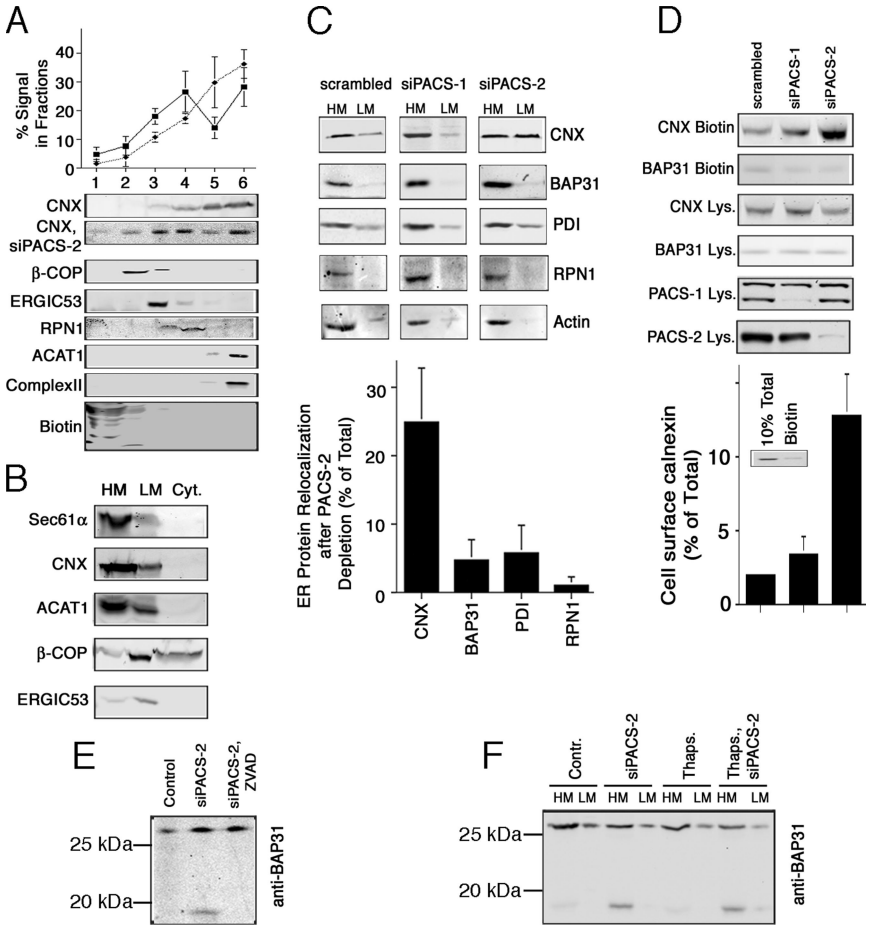

Figure 4. PACS-2–dependent intracellular trafficking of CNX and BAP31. (A) ER and Golgi fractionation upon PACS-2 knockdown. HeLa cells were depleted or not of PACS-2, and cellular membranes were fractionated on a discontinuous Optiprep gradient. Marker proteins indicate cell surface (biotinylated proteins), Golgi (β-COP), ERGIC (ERGIC53), rER (Ribophorin I), MAM (ACAT1), and mitochondria (mitochondrial complex II). Marker proteins were not affected by PACS protein knockdown. The CNX distribution was quantified over four independent experiments. Diamonds and dotted line, control data; squares and solid line, PACS-2 knockdown. $p < 0.05$ for the signal in fractions 5 and 6. (B) Lysate fractionation. HeLa lysates were fractionated into heavy membranes, light membranes, and cytosol; lysates were probed for the indicated markers. (C) CNX and BAP31 membrane fractionation upon PACS-2 knockdown. HeLa cells were depleted or not of PACS-2, and cellular membranes were fractionated into low- and high-speed pellets, which were analyzed by Western blot for CNX, full-length BAP31, PDI, ribophorin I, and actin. We quantified the relocalization of the individual proteins relative to the total signal. Three experiments were quantified. $p < 0.05$ between CNX and all other markers. (D) CNX surface targeting upon PACS-1 and PACS-2 knockdown. HeLa cells were depleted for 2 d of PACS-1 or PACS-2, or were mock-transfected. Biotinylated surface CNX was quantified on Western blots (n = 3). The amount of CNX was expressed as percentage of the total using a 10% total lysates loading control (inset). $p < 0.05$ between siPACS-2 and both other conditions. (E) zVAD-fmk incubation inhibits BAP31p20 formation upon PACS-2 knockdown. Total lysates were probed for full-length BAP31 and BAP31p20. (F) Analysis of BAP31p20 formation upon thapsigargin-induced apoptosis in the presence or absence of PACS-2. HeLa cells were depleted or not of PACS-2, and apoptosis was induced for 16 h with 1 μM thapsigargin. Cellular membranes were fractionated into low- and high-speed pellets, which were analyzed by Western blot for full-length and cleaved BAP31.

of CNX to a juxtanuclear area originated from a reduction of CNX ER retention and a shift to downstream compartments such as the ER-Golgi intermediate compartment (ERGIC) or whether PACS-2 simply altered the intra-ER targeting of CNX. By answering this question we intended to elucidate the significance of PACS-2 for ER targeting and could provide evidence for the existence of a domain-specific ER targeting mechanism.

Our immunofluorescence approach could not unequivocally distinguish between these two possibilities and was unable to quantify the association of CNX with multiple membrane domains in the same cell. Therefore, we switched to biochemical analysis of the CNX/PACS-2 targeting mechanism that allowed us to quantify the amounts of CNX associated with various membranes of the secretory pathway simultaneously. We first examined whether CNX is enriched on any domain of the ER.

For this purpose, we developed a protocol that separates the ER from later secretory compartments and the rER from the MAM on a continuous Optiprep gradient. We fractionated HeLa cellular membranes on this gradient and found surface-biotinylated proteins in fractions 1 and 2 with a peak in fraction 1 (Figure 4A). β-COP, which cosediments with the Golgi complex peaked in fraction 2, whereas the ERGIC marker ERGIC53 peaked in fraction 3. A transmembrane rER marker, ribophorin I, peaked in fraction 4 (Figure 4A). The majority of mitochondrial complex II fractionated into the lowest two fractions of the gradient, as did the ubiquitous MAM marker acyl-CoA: cholesterol acyltransferase 1 (ACAT1, Rusinol *et al.*, 1994; Lee *et al.*, 2000). Using our gradient, we found that CNX sedimented into fractions 3–6, with the majority in fraction 6 under control conditions, thus significantly cofractionating with a MAM marker (Figure 4A). Our results show that PACS-2 knockdown decreased CNX in the MAM fractions from 66 to 42%, but increased its signal in fraction 4, which overlaps best with ribophorin I. The decrease on MAM fractions was statistically significant ($p < 0.05$ for both fractions). Overall, the amount of CNX associated with ER markers decreased from 83 to 69%. This decrease was compensated by a redistribution of CNX to fractions that are enriched for ERGIC53, β-COP, and surface biotinylated proteins (fractions 1–3). The patterns of PDI, ERGIC53, β-COP, and mitochondrial complex II were not altered by PACS-2 silencing (data not shown). Together with our immunofluorescence analysis (Figure 3), our results thus indicate that PACS-2 knockdown had two effects: First, it caused a reduction of CNX on the MAM, but an increase of CNX on the rER. Second, it caused increased recovery of CNX in ERGIC, Golgi and surface fractions, where the CNX signal roughly doubled.

Next, we used a second protocol to complement our Optiprep assays and detect CNX redistribution upon knockdown of PACS proteins by a different method. For this purpose, we separated cellular lysates into a cytosolic fraction, a heavy membrane fraction, and a light membrane fraction by differential centrifugation (Figure 4B). Contrary to the Optiprep gradient, which separates according to a membrane's density, this method separates membranes mostly depending on their size. Our protocol showed that markers of the rER (Sec61α) and MAM markers (ACAT1) fractionate mostly into the heavy membrane pellet, but show some signal in the light membrane pellet. Conversely, markers of the ERGIC and the Golgi (ERGIC-53 and β-COP) fractionate almost exclusively into the light membrane pellet. CNX showed a fractionation pattern that corresponded to rough ER and MAM markers.

Using this fractionation assay, we analyzed homogenates of control HeLa cells and HeLa cells depleted of PACS-1 or PACS-2, respectively. Our results show that PACS-2 knockdown causes a shift of ~25% of the total CNX signal from heavy to light membranes and results in a 50:50 distribution between heavy and light membranes. However, even after PACS-2 knockdown, the CNX fractionation pattern did not resemble the one of a Golgi or ERGIC marker that fractionate mostly into light membranes. Instead, consistent with our Optiprep gradient, PACS-2 knockdown led to an even distribution between heavy and light membranes that is clearly distinct from the ERGIC and coatomer distribution patterns (Figure 4, B and C).

We next sought to confirm if depleting PACS-2 resulted in the appearance of some CNX on the plasma membrane, as suggested by our Optiprep gradient (Figure 4A). Therefore, we analyzed surface targeting of CNX after PACS-1 and PACS-2 siRNA transfection with a surface biotinylation protocol. Total CNX amounts on the surface were calculated using a 10% total lysate loading control and were determined to amount to ~2% of total under steady-state conditions (inset, Figure 4D). Depleting PACS-2, but not PACS-1 led to a sixfold increase of surface CNX (Figure 4D). However, consistent with our fractionation and immunofluorescence results, the surface CNX in the PACS-2–depleted cells amounted to only 12% of total CNX. Together, these results demonstrate how altering PACS-2 expression levels could provide a mechanism for modulating CNX surface amounts.

To examine whether the observed shift to later compartments of the secretory pathway and the plasma membrane was restricted to the PACS-2 interactor CNX, we examined the targeting of three ER markers that overlap to various extents with CNX biochemically. Before PACS-2 knockdown, these marker proteins (BAP31, PDI, and Ribophorin I) showed a similar membrane distribution to CNX. However, none of these markers exhibited a significant shift to lighter membranes (<5% of the total protein for PDI and as little as 1% for Ribophorin I, Figure 4C). Actin, a cytosolic protein also remained unaffected in its membrane association and distribution (Figure 4C). Similar to PDI and as expected from Figure 3, BAP31 showed a minor shift with this fractionation protocol. We also examined surface targeting for BAP31. The BAP31 biotinylation signal was unaffected by either PACS-1 or PACS-2 knockdown (Figure 4D), thus confirming the unresponsiveness of BAP31 to PACS-2 knockdown seen in Figures 3 and 4C.

The fact that BAP31 did not redistribute upon PACS-2 knockdown was surprising, given the fact that this is a demonstrated interactor of CNX (Zuppini *et al.*, 2002). BAP31 is an apoptosis regulatory protein that gives rise to a caspase-generated fragment called BAP31p20 during apoptosis onset, which leads to mitochondria fragmentation (Breckenridge *et al.*, 2003). Full-length BAP31 has a KKEE C-terminal motif that is a COPI-binding consensus motif, whereas BAP31p20 lacks this motif. We thus next examined, whether contrary to full-length BAP31, BAP31p20 showed altered membrane distribution upon PACS-2 knockdown. As shown previously (Simmen *et al.*, 2005), PACS-2 knockdown caused caspase-mediated BAP31p20 formation under resting conditions (Figure 4E), but did not alter the localization of BAP31 significantly (Figure 3). We next examined whether BAP31p20, which lacks most of the cytosolic domain and the COPI motif, remains restricted to heavy membranes of the ER upon PACS-2 knockdown, as full-length BAP31 does. This was indeed the case, regardless of the presence or absence of the apoptosis-inducer thapsigargin (Figure 4E). Therefore, neither cleaved nor full-length BAP31 significantly relocalize after PACS-2 knockdown.

Mutation of the CNX CK2 Sites Modulates PACS-2 Interaction and Amounts on Heavy Membranes

CNX serine phosphorylation by CK2 abrogates efficient binding to PACS-2 (Figure 2B). We thus decided to further test if CNX intracellular targeting depends on PACS-2 with CNX phospho-defective and phospho-mimic mutants. We first assayed binding of these mutants to the thioredoxin-tagged cargo-binding domain of PACS-2 (TRX-PACS-2) and found that GST-CNX does not bind efficiently to the cargo-binding domain of PACS-2, when serines 554 and 564 are mutated to aspartic acids (SSDD, Figure 5A). Conversely, when these serines are mutated to alanines, the binding of the CNX cytosolic domain to PACS-2 was just slightly increased (SSAA in Supplemental Figure S3A and Figure 5A). From these results we would expect SSAA to efficiently reproduce PACS-2–dependent wild-type CNX targeting, whereas SSDD should show reduced retention in the ER and impaired targeting to the MAM.

To examine targeting properties of these CNX mutants, we generated stable cell lines expressing lumenally FLAG-tagged forms of CNX (CNX-FLAG) from CNX knockout mouse embryonic fibroblasts (MEFs; Groenendyk *et al.*, 2006). In these clones, CNX-FLAG wild type and the PACS-2-binding SSAA mutant were found predominantly in the heavy membranes, whereas the CNX-FLAG mutant that cannot bind PACS-2 efficiently showed increased amounts on light membranes (Figure 5B, SSDD). The distributions of the wild-type and SSAA mutant CNX-FLAG were comparable to endogenous CNX found in wild-type MEFs (Figure 5B). This suggested that the SSDD mutation of CNX like the knockdown of PACS-2 caused some CNX to enter the secretory pathway. Confirming these results, when examined by our Optiprep gradient, we detected slightly increased amounts on ERGIC and surface fractions 1–3 for the SSDD mutant. This effect was associated with an equivalent reduction of its signal in the MAM. However, this reduction was only significant in fraction 6 that dropped from 36.5 to 29%. Hence, the effect of the SSDD mutation was considerably less pronounced than the reduction seen with wild-type CNX after PACS-2 knockdown (Figures 4A and 5C). In contrast, the CNX-FLAG SSDD mutant showed a threefold increase of its signal on the surface in our biotinylation assay (Figure 5D), indicating that the PACS-2 motif indeed influences CNX ER targeting to some extent.

We next wanted to determine whether the CNX-FLAG mutants can also reliably reproduce the overlap of endogenous CNX with mitochondria (Figures 1 and 3). For that purpose, we examined the extent of colocalization of their FLAG signal with mitochondria. We found that CNX-FLAG

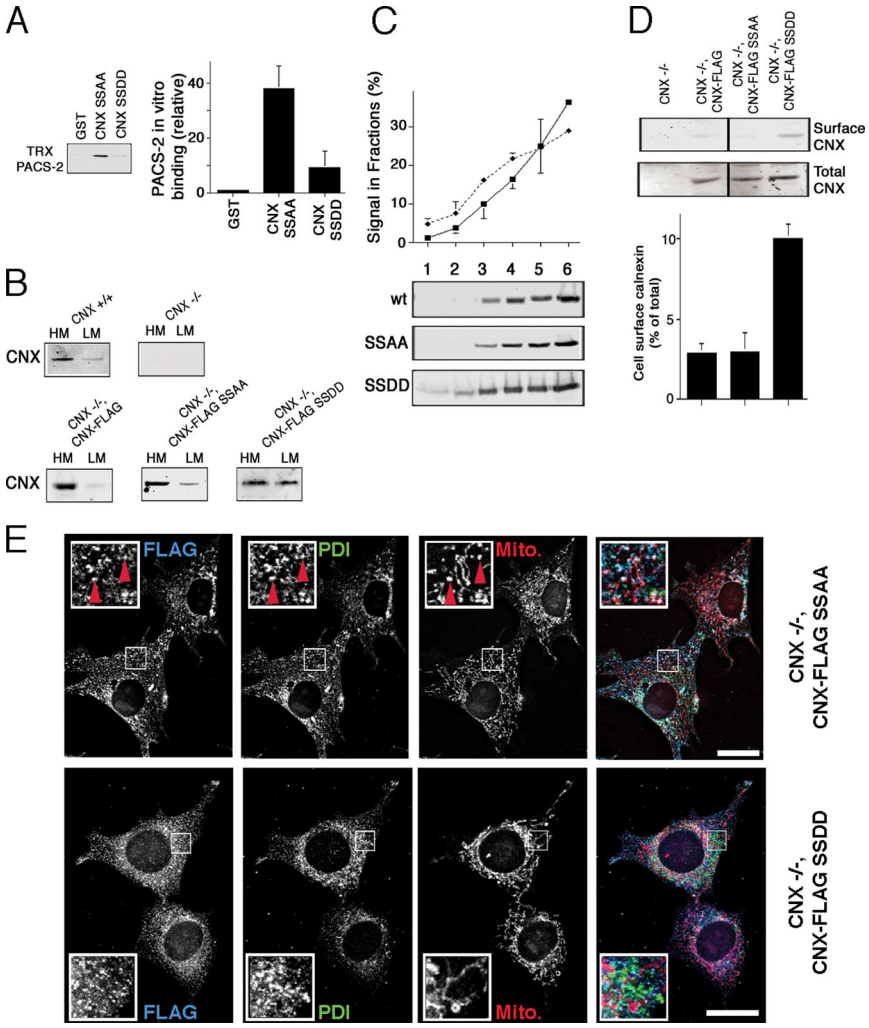

Figure 5. Mutation of the PACS-2–binding motif of CNX. (A) PACS-2–binding motif characterization. Thioredoxin (TRX)-tagged PACS-2 (FBR) was incubated with GST-tagged CNX tail constructs (full-length tail constructs, SSAA = S554,564A,SSDD = S554,564D), and bound GST-tagged molecules were detected by Western blot using anti-GST antibodies. Equal loading was verified by Ponceau staining (data not shown). The intensity of the TRX-PACS-2 signal was quantified and expressed as multiples of the GST signal ($n = 3$). $p = 0.01$ between SSAA and SSDD. (B) Membrane fraction of CNX +/+ and −/− MEF stable transfectants. CNX −/− MEFs stably expressing FLAG-tagged CNX wild-type or SSAA/SSDD mutants were fractionated into heavy and light membranes and analyzed by Western blot for the FLAG (not shown) or the CNX signal. (C) ER and Golgi fractionation of SSAA and SSDD mutants. HeLa cells were transiently transfected with FLAG-tagged CNX wild-type and the SSAA and SSDD mutants. Cellular lysates were fractionated and quantified ($n = 3$) as in Figure 4A on a discontinuous Optiprep gradient. $p < 0.01$ for fraction 6. (D) CNX surface targeting in CNX −/− MEF stable transfectants. CNX −/− MEFs stably expressing FLAG-tagged CNX wild-type or SSAA/SSDD mutants were assayed by biotinylation for surface-targeted FLAG-tagged CNX constructs by Western blot for the FLAG (not shown) or the CNX signal. The line in the gels indicates lanes that were cut out for this presentation. $p < 0.005$ between SSDD and the other constructs. (E) Intracellular localization of CNX CK2 mutants. CNX −/− MEFs stably expressing FLAG-tagged CNX SSAA/SSDD mutants were assayed by immunofluorescence for the localization of the transgene by colocalizing its FLAG signal with endogenous PDI and mitotracker. CNX-FLAG SSAA overlap with PDI and mitochondria is indicated by red arrowheads. Scale bar, 25 μm.

SSAA, like endogenous CNX, showed significant overlap with mitochondria. The localization of this mutant was very similar to endogenous CNX (Figure 5E, top row; compare to Figure 3A). As observed for wild-type endogenous CNX, we observed numerous areas of overlap between the FLAG, the PDI and mitochondrial staining (indicated by red arrowheads). In contrast, it was unclear whether the phosphomimic CNX-FLAG SSDD mutant showed reduced overlap with mitochondria (Figure 5E, bottom row). Its reticular staining was evenly distributed throughout the cytosol. Interestingly, while giving a biochemical distribution that resembled wild-type CNX after PACS-2 knockdown, this phospho-mimic mutant did not reproduce the juxtanuclear staining pattern (Figure 3E). We address this discrepancy in the discussion.

PACS-2 Connects CNX to Coatomer

PACS proteins connect cytosolic acidic motifs of cargo proteins to sorting coats; for example, PACS-1 connects furin to AP-1, and PACS-2 connects polycystin-2 to coatomer (COPI; Crump *et al.*, 2001; Kottgen *et al.*, 2005). Together, PACS proteins form a characteristic ternary complex with their cargo proteins and coat complexes. We therefore tested whether CNX, PACS-2 and coatomer can also form such a ternary complex. We incubated COPI with thioredoxin-tagged PACS-2 or GST-tagged CNX, or the two together. Because GST-tagged CNX was able to capture four times more COPI in the presence of PACS-2, CNX, PACS-2 and COPI are indeed able to form a ternary complex (Figure 6A). We next wanted to compare the influence of COPI on intracellular routing of CNX and BAP31 to the one exerted by PACS-2. Similar to PACS-2 knockdown, COPI knockdown caused an increase of CNX on the cell surface, when cells were analyzed after 2 d of siRNA transfection. Interestingly and consistent with the presence of a COPI-binding motif on the C-terminus of BAP31, we also observed a minor increase of cell surface BAP31 (Figure 6B). However, COPI knockdown, but not PACS-2 knockdown caused some cell death that we detected with the appearance of active caspase-3 (Supplemental Figure S1B), thus potentially allowing some intracellular proteins to be biotinylated. We were able to confirm the COPI-dependent effects using the LDLf cell line, which degrades ε-COP in a temperature-sensitive way (Guo *et al.*, 1994). When this mutant CHO cell line was shifted from 34 to 40°C for 6 h, we observed an increase of the cell surface amounts of both CNX and BAP31 (Figure 6C). Their amounts on the plasma membrane increased more in this experiment, likely due to incomplete knockdown of β-COP using siRNA (Figure 6B).

We confirmed the relocalization of CNX and BAP31 upon 2 d siRNA β-COP knockdown by immunofluorescence (Figure 6D). Again, in contrast to PACS-2 knockdown (Figure 3),

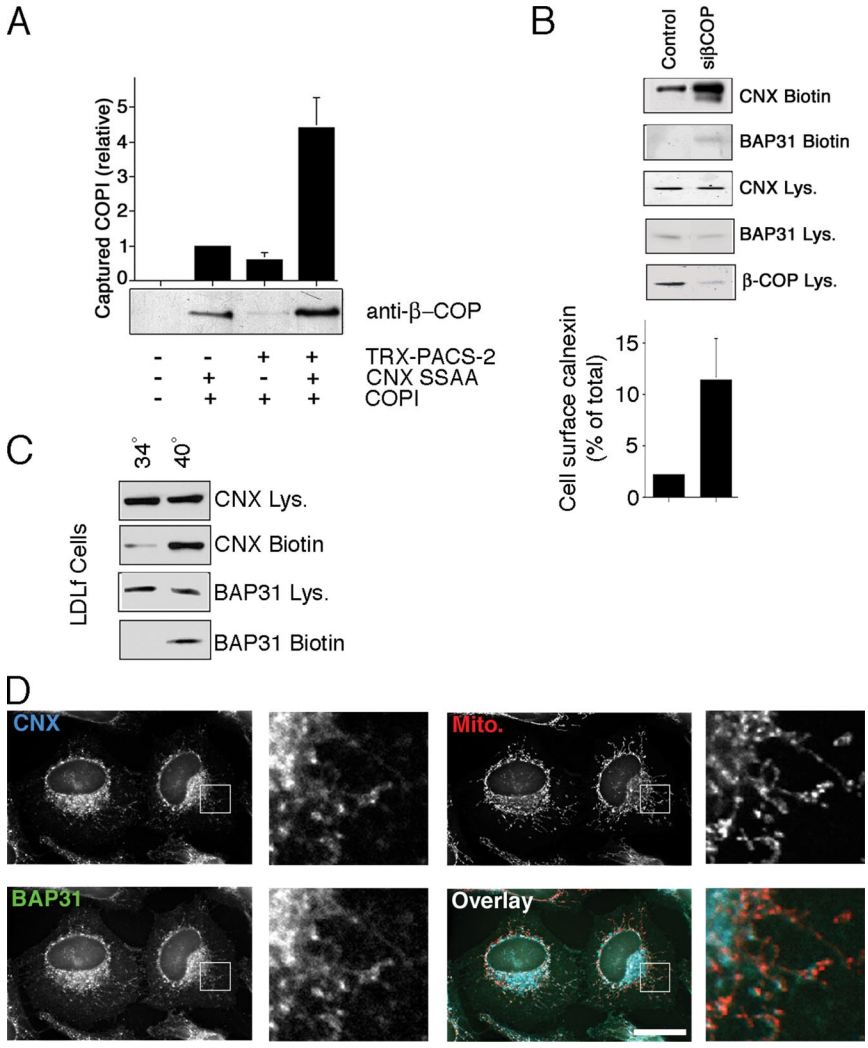

Figure 6. CNX and BAP31 depend on coatomer for their intracellular localization. (A) Ternary complex formation between purified COPI, PACS-2, and CNX. Signal corresponds to β-COP immobilized by GST-CNX S554,564A in the presence or absence of TRX-tagged PACS-2FBR. (B) Cell surface CNX and BAP31 upon COPI knockdown. HeLa control cells or cells depleted of β-COP were assayed for cell surface CNX and BAP31. The relative amount of cell surface CNX was quantified (n = 3). $p < 0.05$ between siPACS-2 and other conditions. (C) Cell surface CNX and BAP31 in LDLf cells (temperature-sensitive for ε-COP). LDLf cells were incubated at 34°C (permissive temperature) or at 40°C (causing loss of ε-COP) and assayed for cell surface CNX and BAP31. (D) Intracellular localization of CNX and BAP31 upon COPI knockdown. HeLa cells depleted of β-COP were assayed for immunofluorescence localization of CNX and BAP31. β-COP–depleted cells were identified by Golgi dispersal and CNX restriction. Scale bar, 25 μm.

both CNX and BAP31 clustered in the juxtanuclear area. Together, these findings suggest that PACS-2 and COPI do not have the same levels of control on CNX and BAP31 for their intracellular localization. Although both CNX and BAP31 depend on COPI for their intracellular localization, PACS-2 provides a specific mechanism for CNX that results in the normal steady-state distribution of this chaperone along the secretory pathway and within the ER.

DISCUSSION

The ER is emerging as one of the most complex cellular organelles, performing a multitude of functions ranging from protein synthesis, protein folding, protein degradation, glycosylation, lipid synthesis, lipid transfer, calcium signaling, and calcium storage, to name but a few. Not unexpectedly, this multifunctional organelle comprises multiple domains, but sorting signals and proteins that regulate the intra-ER distribution of proteins are unknown. Our results now show that CNX is enriched at the MAM, a finding that was recently suggested by Hayashi and Su (2007). Our results also show that PACS-2 is a factor that contributes to the enrichment of CNX on the MAM.

The knockdown of PACS-2 interferes with correct CNX targeting in multiple ways. First, it shifts CNX from peripheral ER tubules overlapping with mitochondria to a sharp juxtanuclear localization (Figure 3). This shift also corresponds to a reduction of overlap between CNX and mitochondria, as shown by immunofluorescence and fractionation (Figures 3 and 4A). Second, PACS-2 knockdown causes limited CNX redistribution from ER membrane fractions to membrane fractions enriched with markers of the ERGIC and Golgi complex, as suggested by our fractionation and differential centrifugation assays (Figures 4, A and C). Third, PACS-2 knockdown increases CNX levels on the cell surface as observed by a biotinylation assay and our Optiprep fractionation, although both methods show that the majority of CNX remains intracellular (Figure 4, A and D). Taken together, PACS-2 regulates the amounts of CNX on the MAM and on the rER. PACS-2 also retains CNX within the ER and prevents appearance of CNX in biochemical fractions that contain the ERGIC, the Golgi, and on the plasma membrane. The regulatable interaction between PACS-2 and CNX could therefore account for increased amounts of CNX on the plasma membrane of certain cell types (Wiest *et al.*, 1995).

Several models can explain our observations: PACS-2 could be directly regulating the amounts of CNX on the MAM (see also below for further discussion). In this case, the loss of intra-ER targeting would initially lead to a non-

restricted distribution within the ER, which could overwhelm the ER retention mechanism somewhat, leading to a relative enrichment at ER exit sites. Alternatively, PACS-2 could simply regulate CNX ER retention at or after ER exit sites. Loss of PACS-2 would then cause CNX to leak from the ER, which would eventually also cause a loss of MAM-localized CNX. In agreement with this model, PACS-2 also interacts with COPI, suggesting that COPI and PACS-2 cooperate to retain CNX within the ER. The mechanism that the two proteins utilize for this retention could very well be retrieval, as shown previously for COPI itself (Letourneur *et al.,* 1994). An unexplored possibility is that PACS-2 also interacts with other components of the ER sorting and trafficking machinery, such as COPII.

To shed some more light on the PACS-2 mediated trafficking of CNX, we examined CNX phosphomimic mutants. Whereas the constitutively PACS-2-binding SSAA mutant nicely reproduced the staining and membrane fractionation of wild-type CNX, the SSDD mutant showed reduced binding to PACS-2, but was not as mislocalized as might be expected. Our data shows that this mutant showed some leakage into Optiprep fractions that are enriched for markers of the cell surface and the ERGIC (Figure 5, B and D). This mutant also showed significantly reduced sedimentation into the very bottom fraction of the ER that contains the MAM marker ACAT1 (Figure 5C). When examined by immunofluorescence staining, this mutant did, however, not reproduce the sharp gradient around the nucleus that is seen with PACS-2 knockdown (compare Figure 3E with 5E). Several reasons can lead to this behavior: First, the SSDD mutant shows significantly reduced, but not abolished, binding to PACS-2 (Figure 5A). Second, phospho-mimic CNX is still able to interact with ribosomes, an interaction that leads to ER retention (Chevet *et al.,* 1999). Third, PACS-2 knockdown is expected to lead to reduced, but not abolished binding of CNX to COPI (Figure 6A), and could hence result in a partial rescue of retrieval by COPI.

Hence, it appears that although the phosphorylation by CK2 promotes CNX's association with ribosomes (Chevet *et al.,* 1999), its dephosphorylation promotes interaction of CNX with PACS-2 and targeting to heavy ER membranes, including the MAM, as shown here. Both studies together suggest an equilibrium of phosphorylated and nonphosphorylated CNX inside the ER that establishes wild-type CNX steady-state distribution between the rER and the MAM.

Both CNX and BAP31 show COPI dependence for their ER retention. Interestingly, neither the interference with COPI, nor the interference with PACS-2, nor the combination of the two (data not shown) leads to a complete release of either protein from the ER. These observations suggest that CNX is retained within the ER by multiple mechanisms. They also demonstrate that while PACS-2 *contributes* to CNX ER retention, PACS-2 is not the *sole* factor for CNX ER retention. What additional mechanisms could retain CNX in the ER? It is likely that the lumenal domain of CNX contributes to its intracellular retention. One possibility could be thiol-mediated retention, because CNX has two disulfide bonds: Cys161-Cys195 in its globular domain and Cys361-Cys367 in the arm (Schrag *et al.,* 2001; Anelli *et al.,* 2003). However, β-mercaptoethanol, typically used to release proteins retained in the ER by this mechanism has no effect on the amount of CNX on the cell surface (Supplemental Figure S3B). Another possible ER retention mechanism could be the association of CNX with newly synthesized proteins in the rough ER, also mediated by the CNX luminal domain. However, tunicamycin treatment for 10 h, which abolishes interaction of CNX with these substrates actually decreases the amount of CNX on the cell surface (Okazaki *et al.,* 2000). Together, this suggests that other, yet unknown mechanisms additionally retain CNX inside the ER.

Although the localization of CNX to the vicinity of ribosomes stems from its role in protein folding, it is less obvious why CNX might be found in the vicinity of mitochondria and on the MAM (Figures 1, 3, 4, and 5). Two functions of CNX have been reported that suggest an important role for this chaperone on the MAM. On the one hand, CNX acts as a chaperone for the IP_3R that is found on the MAM (Joseph *et al.,* 1999). Furthermore, CNX interacts with the SERCA2b calcium pump that is also found on the MAM (Roderick *et al.,* 2000; Szabadkai *et al.,* 2006). This interaction regulates intracellular calcium oscillation, dependent on CNX phosphorylation. In principle, this finding could implicate the interaction of CNX with PACS-2 in this mechanism. However, serine 583 on CNX, which regulates the calcium oscillations, is distinct from the PACS-2-binding acidic cluster (Roderick *et al.,* 2000). Our results therefore rather suggest a role for PACS-2 in shuttling CNX between ER domains or in providing adequate ER retention that would result in the steady-state enrichment of CNX on the MAM (Figure 4A).

PACS-2 is found on or in the vicinity of mitochondria (Figure 1; Simmen *et al.,* 2005). PACS-2 not only influences the amounts of CNX on the MAM, but also of some lipid transfer proteins (Simmen *et al.,* 2005). Because the proteins in this latter group do not exhibit any obvious acidic cluster motifs, PACS-2 might influence the formation of and targeting to MAMs by localizing a "master" MAM protein. However, contradicting this idea are our findings that BAP31 does not leave the ER and maintains a heavy membrane association (Figures 3 and 4, C and D). Furthermore, even BAP31p20 that lacks a COPI binding motif remains associated with the MAM upon PACS-2 knockdown (Figure 4F). Together, our data suggest that PACS-2 influences targeting to MAMs in a more complex way than initially thought.

Clearly, however, our results demonstrate the specificity of PACS-2–mediated sorting of CNX along the secretory pathway, which depends on an acidic, phosphorylatable cluster. They also agree with recent studies that report a role of PACS-2 in the early endosome-to-TGN sorting of the CI-MPR and in the ability of HIV-1 Nef to down-regulate cell surface MHC I, because both depend on similar consensus sequences (Atkins *et al.,* 2008). Our findings are thus at odds with the data presented in Lubben *et al.* (2007), which led to the conclusion that PACS proteins are ". . . dispensable for the sorting of cargo proteins with acidic cluster motifs."

As with the binding of furin to PACS-1 and PACS-2, protein kinase CK2 regulates binding of CNX to PACS-2. When analyzing all known interactors of PACS proteins, PACS-2 appears to exhibit a preference, but not a requirement for dephosphorylated cargo proteins, as exemplified by Bid and CNX (this study and Simmen *et al.,* 2005). Interestingly, this characteristic of the PACS-2/cargo binding resembles the regulation of ER forward transport by 14-3-3 proteins, which is also regulated by the phosphorylation state of cargo proteins (Mrowiec and Schwappach, 2006). PACS-2 and the 14-3-3 proteins have opposing roles for ER retention: whereas PACS-2 promotes ER retention by forming a ternary cargo/COPI complex, the 14-3-3 proteins compete with COPI for cargo binding and allow their exit from the ER upon interaction (O'Kelly *et al.,* 2002; Vivithanaporn *et al.,* 2006). It will be interesting to determine whether PACS-2 and 14-3-3 proteins interact functionally and/or physically to regulate ER retention, together with COPI. Also, it will be of interest to determine an involvement of

14-3-3 proteins in the intra-ER localization of CNX, besides the known involvement of COPI (Rajagopalan *et al.*, 1994).

One of our most intriguing findings concerns the cleavage of BAP31 upon PACS-2 knockdown. What could be the explanation for this phenomenon? Because zVAD-fmk inhibits this cleavage, caspases are presumably involved in the formation of BAP31p20 upon PACS-2 knockdown. Therefore, insufficient PACS-2 on the ER might trigger the activation of caspases. This effect could be originating from the observed ER stress upon PACS-2 knockdown (Simmen *et al.*, 2005) or from the missorting of CNX away from the ER (this study). However, because PACS-2 knockdown eventually blocks the onset of apoptosis and does not lead to the activation of downstream caspases, our results exclude the possibility that the knockdown of PACS-2 is simply toxic.

BAP31p20 has been proposed to have proapoptotic activity through activation of Drp-1, which causes the fragmentation of mitochondria. The consequence of the activation of Drp1 is so far unclear, as this may either promote or inhibit apoptosis induction (Breckenridge *et al.*, 2003; Szabadkai *et al.*, 2004). Our results now suggest that BAP31p20 formation is indeed not sufficient to trigger apoptosis, but that this molecule requires PACS-2 to do so. This contrasts with the localization of BAP31 and BAP31p20, which does not depend significantly on PACS-2.

Together, our results propose two distinct roles of PACS-2 for the correct functioning of the ER: on the one hand, it retains in collaboration with coatomer a subset of ER proteins with acidic cytosolic clusters on domains of the ER, including the MAM, but on the other hand, PACS-2 is also required for the induction of apoptosis. Whether this latter function is limited to the sorting of dephosphorylated Bid onto mitochondria, as shown previously (Simmen *et al.*, 2005) remains to be tested.

ACKNOWLEDGMENTS

We thank Sarah Hughes for advice with coimmunoprecipitation, Andrew Simmonds for assistance with confocal microscopy, and Rick Rachubinski for providing lab space during the initial stages of this project. We thank Rainer Duden (Royal Holloway, University of London) for purified coatomer. We also especially thank Marek Michalak (University of Alberta) for providing us with CNX wild-type and knockout MEFs. We thank Michael Bui for technical assistance and Paul Melançon for critical reading of this manuscript. This work was supported by Swiss National Science Foundation Fellowship PA00A-101489, National Cancer Institute of Canada Grant 17291 and Alberta Heritage Foundation for Medical Research Grant 200500396 (T.S.) and National Institutes of Health Grants DK37274 and AI49793 (G.T.). This research was supported by the Terry Fox Foundation.

REFERENCES

Anelli, T., Alessio, M., Bachi, A., Bergamelli, L., Bertoli, G., Camerini, S., Mezghrani, A., Ruffato, E., Simmen, T., and Sitia, R. (2003). Thiol-mediated protein retention in the endoplasmic reticulum: the role of ERp44. EMBO J. *22*, 5015–5022.

Annaert, W. G., Becker, B., Kistner, U., Reth, M., and Jahn, R. (1997). Export of cellubrevin from the endoplasmic reticulum is controlled by BAP31. J. Cell Biol. *139*, 1397–1410.

Arap, M. A., Lahdenranta, J., Mintz, P. J., Hajitou, A., Sarkis, A. S., Arap, W., and Pasqualini, R. (2004). Cell surface expression of the stress response chaperone GRP78 enables tumor targeting by circulating ligands. Cancer Cell *6*, 275–284.

Atkins, K. M., Thomas, L., Youker, R. T., Harriff, M. J., Pissani, F., You, H., and Thomas, G. (2008). HIV-1 NEF binds PACS-2 to assemble a multi-kinase cascade that triggers MHC-I downregulation: analysis using siRNA and knockout mice. J. Biol. Chem. *283*, 11772–11784.

Borgese, N., Francolini, M., and Snapp, E. (2006). Endoplasmic reticulum architecture: structures in flux. Curr. Opin. Cell Biol. *18*, 358–364.

Breckenridge, D. G., Stojanovic, M., Marcellus, R. C., and Shore, G. C. (2003). Caspase cleavage product of BAP31 induces mitochondrial fission through endoplasmic reticulum calcium signals, enhancing cytochrome c release to the cytosol. J. Cell Biol. *160*, 1115–1127.

Chen, W., and Helenius, A. (2000). Role of ribosome and translocon complex during folding of influenza hemagglutinin in the endoplasmic reticulum of living cells. Mol. Biol. Cell *11*, 765–772.

Chevet, E., Wong, H. N., Gerber, D., Cochet, C., Fazel, A., Cameron, P. H., Gushue, J. N., Thomas, D. Y., and Bergeron, J. J. (1999). Phosphorylation by CK2 and MAPK enhances calnexin association with ribosomes. EMBO J. *18*, 3655–3666.

Crump, C. M., Xiang, Y., Thomas, L., Gu, F., Austin, C., Tooze, S. A., and Thomas, G. (2001). PACS-1 binding to adaptors is required for acidic cluster motif-mediated protein traffic. EMBO J. *20*, 2191–2201.

Duden, R. (2003). ER-to-Golgi transport: COP I and COP II function (Review). Mol. Membr. Biol. *20*, 197–207.

Feliciangeli, S. F., Thomas, L., Scott, G. K., Subbian, E., Hung, C. H., Molloy, S. S., Jean, F., Shinde, U., and Thomas, G. (2006). Identification of a pH sensor in the furin propeptide that regulates enzyme activation. J. Biol. Chem. *281*, 16108–16116.

Frenkel, Z., Shenkman, M., Kondratyev, M., and Lederkremer, G. Z. (2004). Separate roles and different routing of calnexin and ERp57 in endoplasmic reticulum quality control revealed by interactions with asialoglycoprotein receptor chains. Mol. Biol. Cell *15*, 2133–2142.

Gagnon, E., Duclos, S., Rondeau, C., Chevet, E., Cameron, P. H., Steele-Mortimer, O., Paiement, J., Bergeron, J. J., and Desjardins, M. (2002). Endoplasmic reticulum-mediated phagocytosis is a mechanism of entry into macrophages. Cell *110*, 119–131.

Goetz, J. G., Genty, H., St-Pierre, P., Dang, T., Joshi, B., Sauve, R., Vogl, W., and Nabi, I. R. (2007). Reversible interactions between smooth domains of the endoplasmic reticulum and mitochondria are regulated by physiological cytosolic Ca^{2+} levels. J. Cell Sci. *120*, 3553–3564.

Groenendyk, J., Zuppini, A., Shore, G., Opas, M., Bleackley, R. C., and Michalak, M. (2006). Caspase 12 in calnexin-deficient cells. Biochemistry *45*, 13219–13226.

Guo, Q., Vasile, E., and Krieger, M. (1994). Disruptions in Golgi structure and membrane traffic in a conditional lethal mammalian cell mutant are corrected by epsilon-COP. J. Cell Biol. *125*, 1213–1224.

Hayashi, T., and Su, T. P. (2007). Sigma-1 receptor chaperones at the ER-mitochondrion interface regulate Ca(2+) signaling and cell survival. Cell *131*, 596–610.

Higo, T., Hattori, M., Nakamura, T., Natsume, T., Michikawa, T., and Mikoshiba, K. (2005). Subtype-specific and ER lumenal environment-dependent regulation of inositol 1,4,5-trisphosphate receptor type 1 by ERp44. Cell *120*, 85–98.

John, L. M., Lechleiter, J. D., and Camacho, P. (1998). Differential modulation of SERCA2 isoforms by calreticulin. J. Cell Biol. *142*, 963–973.

Joseph, S. K., Boehning, D., Bokkala, S., Watkins, R., and Widjaja, J. (1999). Biosynthesis of inositol trisphosphate receptors: selective association with the molecular chaperone calnexin. Biochem. J. *342*(Pt 1), 153–161.

Kamhi-Nesher, S., Shenkman, M., Tolchinsky, S., Fromm, S. V., Ehrlich, R., and Lederkremer, G. Z. (2001). A novel quality control compartment derived from the endoplasmic reticulum. Mol. Biol. Cell *12*, 1711–1723.

Kottgen, M. *et al.* (2005). Trafficking of TRPP2 by PACS proteins represents a novel mechanism of ion channel regulation. EMBO J. *24*, 705–716.

Lee, R. G., Willingham, M. C., Davis, M. A., Skinner, K. A., and Rudel, L. L. (2000). Differential expression of ACAT1 and ACAT2 among cells within liver, intestine, kidney, and adrenal of nonhuman primates. J. Lipid Res. *41*, 1991–2001.

Letourneur, F., Gaynor, E. C., Hennecke, S., Demolliere, C., Duden, R., Emr, S. D., Riezman, H., and Cosson, P. (1994). Coatomer is essential for retrieval of dilysine-tagged proteins to the endoplasmic reticulum. Cell *79*, 1199–1207.

Levine, T., and Loewen, C. (2006). Inter-organelle membrane contact sites: through a glass, darkly. Curr. Opin. Cell Biol. *18*, 371–378.

Lubben, N. B., Sahlender, D. A., Motley, A. M., Lehner, P. J., Benaroch, P., and Robinson, M. S. (2007). HIV-1 Nef-induced down-regulation of MHC class I requires AP-1 and clathrin but not PACS-1, and is impeded by AP-2. Mol. Biol. Cell *18*, 3351–3365.

Mezghrani, A., Courageot, J., Mani, J. C., Pugniere, M., Bastiani, P., and Miquelis, R. (2000). Protein-disulfide isomerase (PDI) in FRTL5 cells. pH-dependent thyroglobulin/PDI interactions determine a novel PDI function in the post-endoplasmic reticulum of thyrocytes. J. Biol. Chem. *275*, 1920–1929.

Michelsen, K., Yuan, H., and Schwappach, B. (2005). Hide and run. EMBO Rep. *6*, 717–722.

Misra, U. K., Deedwania, R., and Pizzo, S. V. (2006). Activation and cross-talk between Akt, NF-kappaB, and unfolded protein response signaling in 1-LN prostate cancer cells consequent to ligation of cell surface-associated GRP78. J. Biol. Chem. *281*, 13694–13707.

Mrowiec, T., and Schwappach, B. (2006). 14-3-3 proteins in membrane protein transport. Biol. Chem. *387*, 1227–1236.

O'Kelly, I., Butler, M. H., Zilberberg, N., and Goldstein, S. A. (2002). Forward transport. 14-3-3 binding overcomes retention in endoplasmic reticulum by dibasic signals. Cell *111*, 577–588.

Okazaki, Y., Ohno, H., Takase, K., Ochiai, T., and Saito, T. (2000). Cell surface expression of calnexin, a molecular chaperone in the endoplasmic reticulum. J. Biol. Chem. *275*, 35751–35758.

Rajagopalan, S., Xu, Y., and Brenner, M. B. (1994). Retention of unassembled components of integral membrane proteins by calnexin. Science *263*, 387–390.

Rizzuto, R., Pinton, P., Carrington, W., Fay, F. S., Fogarty, K. E., Lifshitz, L. M., Tuft, R. A., and Pozzan, T. (1998). Close contacts with the endoplasmic reticulum as determinants of mitochondrial Ca^{2+} responses. Science *280*, 1763–1766.

Roderick, H. L., Lechleiter, J. D., and Camacho, P. (2000). Cytosolic phosphorylation of calnexin controls intracellular Ca(2+) oscillations via an interaction with SERCA2b. J. Cell Biol. *149*, 1235–1248.

Rusinol, A. E., Cui, Z., Chen, M. H., and Vance, J. E. (1994). A unique mitochondria-associated membrane fraction from rat liver has a high capacity for lipid synthesis and contains pre-Golgi secretory proteins including nascent lipoproteins. J. Biol. Chem. *269*, 27494–27502.

Schermer, B. *et al.* (2005). Phosphorylation by casein kinase 2 induces PACS-1 binding of nephrocystin and targeting to cilia. EMBO J. *24*, 4415–4424.

Schrag, J. D., Bergeron, J. J., Li, Y., Borisova, S., Hahn, M., Thomas, D. Y., and Cygler, M. (2001). The structure of calnexin, an ER chaperone involved in quality control of protein folding. Mol. Cell *8*, 633–644.

Scott, G. K., Fei, H., Thomas, L., Medigeshi, G. R., and Thomas, G. (2006). A PACS-1, GGA3 and CK2 complex regulates CI-MPR trafficking. EMBO J. *25*, 4423–4435.

Simmen, T. *et al.* (2005). PACS-2 controls endoplasmic reticulum-mitochondria communication and Bid-mediated apoptosis. EMBO J. *24*, 717–729.

Simmen, T., Nobile, M., Bonifacino, J. S., and Hunziker, W. (1999). Basolateral sorting of furin in MDCK cells requires a phenylalanine-isoleucine motif together with an acidic amino acid cluster. Mol. Cell Biol. *19*, 3136–3144.

Spiliotis, E. T., Manley, H., Osorio, M., Zuniga, M. C., and Edidin, M. (2000). Selective export of MHC class I molecules from the ER after their dissociation from TAP. Immunity *13*, 841–851.

Szabadkai, G., Bianchi, K., Varnai, P., De Stefani, D., Wieckowski, M. R., Cavagna, D., Nagy, A. I., Balla, T., and Rizzuto, R. (2006). Chaperone-mediated coupling of endoplasmic reticulum and mitochondrial Ca^{2+} channels. J. Cell Biol. *175*, 901–911.

Szabadkai, G., Simoni, A. M., Chami, M., Wieckowski, M. R., Youle, R. J., and Rizzuto, R. (2004). Drp-1-dependent division of the mitochondrial network blocks intraorganellar Ca^{2+} waves and protects against Ca^{2+}-mediated apoptosis. Mol. Cell *16*, 59–68.

Teasdale, R. D., and Jackson, M. R. (1996). Signal-mediated sorting of membrane proteins between the endoplasmic reticulum and the golgi apparatus. Annu. Rev. Cell Dev. Biol. *12*, 27–54.

Vance, J. E. (1990). Phospholipid synthesis in a membrane fraction associated with mitochondria. J. Biol. Chem. *265*, 7248–7256.

Vivithanaporn, P., Yan, S., and Swanson, G. T. (2006). Intracellular trafficking of KA2 kainate receptors mediated by interactions with coatomer protein complex I (COPI) and 14-3-3 chaperone systems. J. Biol. Chem. *281*, 15475–15484.

Wakana, Y., Takai, S., Nakajima, K. I., Tani, K., Yamamoto, A., Watson, P., Stephens, D. J., Hauri, H. P., and Tagaya, M. (2008). Bap31 is an itinerant protein that moves between the peripheral ER and a juxtanuclear compartment related to ER-associated degradation. Mol. Biol. Cell. *19*, 1825–1836.

Wan, L., Molloy, S. S., Thomas, L., Liu, G., Xiang, Y., Rybak, S. L., and Thomas, G. (1998). PACS-1 defines a novel gene family of cytosolic sorting proteins required for trans-Golgi network localization. Cell *94*, 205–216.

Wiest, D. L., Burgess, W. H., McKean, D., Kearse, K. P., and Singer, A. (1995). The molecular chaperone calnexin is expressed on the surface of immature thymocytes in association with clonotype-independent CD3 complexes. EMBO J. *14*, 3425–3433.

Wong, H. N., Ward, M. A., Bell, A. W., Chevet, E., Bains, S., Blackstock, W. P., Solari, R., Thomas, D. Y., and Bergeron, J. J. (1998). Conserved in vivo phosphorylation of calnexin at casein kinase II sites as well as a protein kinase C/proline-directed kinase site. J. Biol. Chem. *273*, 17227–17235.

Zen, K., Utech, M., Liu, Y., Soto, I., Nusrat, A., and Parkos, C. A. (2004). Association of BAP31 with CD11b/CD18. Potential role in intracellular trafficking of CD11b/CD18 in neutrophils. J. Biol. Chem. *279*, 44924–44930.

Zuppini, A., Groenendyk, J., Cormack, L. A., Shore, G., Opas, M., Bleackley, R. C., and Michalak, M. (2002). Calnexin deficiency and endoplasmic reticulum stress-induced apoptosis. Biochemistry *41*, 2850–2858.